A Qualitative Assessment of Microclimatic Perturbations in a Tunnel

Rohit Salve[1], Nir Y. Krakauer[2], Michael B. Kowalsky[1] and Stefan Finsterle[1]

[1]*Earth Sciences Division, Lawrence Berkeley National Laboratory,*

1 Cyclotron Road

MS-1116, Berkeley CA 94720

[2]*Department of Earth and Planetary Sciences*

University of California, Berkeley, CA 94720

Phone: 510 486 6416

Fax: 510 486 6608

Email: R_Salve@lbl.gov

JOC-07-0067.R1

Abstract

Understanding microclimate dynamics in tunnels is important for designing, operating, and maintaining underground facilities. For example, for the geological disposal of radioactive materials, condensation of vapor should be minimized as liquid water can accelerate waste package corrosion and radionuclide release. While microclimate dynamics are known to be dominated by the advection of heat and moisture, additional factors may also be important, such as the presence of fractures or faults. We present data collected using a relatively inexpensive method that is under development to assess microclimatic perturbations underground. By combining standard temperature and relative humidity sensors with low-cost sensors designed to detect changes in water content, we were able to infer microclimate dynamics along a tunnel at the proposed geological repository at Yucca Mountain, Nevada. We observed significant differences in the pattern of condensation in a faulted zone relative to that of a nonfaulted zone, suggesting that hydrogeologic features have to be accounted for when evaluating the microclimate dynamics of excavated cavities in fractured, partially saturated rocks.

Key Words

Microclimate, Tunnels, Condensation, Evaporation, Fractured Rock, Monitoring Techniques

I. Introduction

An understanding of microclimate dynamics in underground cavities is important for applications ranging from the design of waste disposal facilities to the preservation of artifacts or fauna in caves (De Freitas and Schmekal, 2003). In such environments, which typically have high humidity and contain partially saturated rocks, the microclimate is dominated by advection of heat and moisture (De Freitas and Littlejohn, 1987), with the thermal state being defined by the geothermal flux, thermal diffusion from the surface, water circulation, and air exchange with the outside atmosphere (Crouzeix et al., 2003).

At the proposed geological repository for radioactive waste at Yucca Mountain, Nevada, it is crucial to minimize water exposure of waste containers emplaced in horizontal tunnels (drifts). The presence of in-drift water caused by seepage from the surrounding rock mass or by condensation of vapor can accelerate waste package corrosion and potentially enhance radionuclide dissolution, release, and transport through the geosphere. It is important to understand the microclimates that could develop in this fractured and faulted rock environment as they affect the propensity for water condensation.

Yucca Mountain is located in the central portion of the southern Basin and Range, which resulted from late Cenozoic extensional faulting (Piety, 1996). Key features in the structural geology of the region include block-bounding faults, occurring every 1–4 km, and intrablock faults (Stuckless and Dudley, 2002). Because the proposed geological repository will include kilometers of horizontal tunnels, it will inevitably be intercepted by near-vertical faults.

Here we present data collected using a relatively inexpensive technique being developed to monitor microclimate dynamics. Using sensors designed to detect changes in water saturation caused by condensation and evaporation, we were able to monitor in-drift microclimate dynamics at higher temporal and spatial resolution than previously investigated (to our knowledge). We observed significant differences between and within faulted and nonfaulted zones. Given the importance of evaporation and condensation on the performance of underground facilities, it is essential to have a detailed understanding of the in-drift microclimate and the factors that affect its dynamics. High-resolution monitoring of moisture conditions is essential to evaluate the impact of hydrogeological features on in-drift microclimate dynamics.

II. Study Site

A high-resolution moisture monitoring study was conducted over a period of 14 months, beginning in late 2001, in the immediate vicinity of the Solitario Canyon Fault Zone (SCFZ) at Yucca Mountain (Figure 1). The SCFZ, considered to be the most laterally continuous fault at Yucca Mountain, is accessible ~300 m below ground surface through a 2.7 km long, 5 m diameter tunnel, the Cross Drift (CD). The CD, excavated in 1998, is located within the Topopah Spring Tuff (Figure 1a). The eastern strand of the SCFZ begins at Station 25+85, though the influence of the SCFZ on the surrounding rock extends to Station 25+00 in the form of shear intensity (Mongano et al., 1999). (Station numbers refer to distance in meters, with 25+85, for example, indicating the location 2,585 m from the start of the CD).

III. Methods

a. Isolation of the CD from engineered ventilation

During the six-month excavation of the CD, forced ventilation was maintained by a series of fans in a ~1 m diameter tube that circulated air along the entire length of the tunnel. The impact of the engineered ventilation on the in-drift microclimate was substantial, and thus had to be mitigated for this investigation by isolating four sections in the terminal portion of the CD with steel doors, referred to as bulkheads, at Station 17+63, 22+00, 25+03, and 26+00 (Figure 1b). The first two sections were outside the SCFZ: between Station 17+63 and 22+00 (Section 1), and between Station 22+00 and 25+03 (Section 2). The third section (Section 3) was located between Station 25+03 and 26+00 and included the eastern strand of the Solitario Canyon Fault. The fourth section (Section 4) was located beyond Station 26+00 in a faulted zone between the eastern and western strands of the Solitario Canyon Fault. This configuration allowed us to monitor microclimate dynamics outside (Sections 1 and 2) and within (Sections 3 and 4) the SCFZ.

On November 19, 2001, the ventilation was stopped in Sections 2–4, and these sections were sealed by closing the last three bulkhead doors. One month later, Section 1 was similarly sealed by closing the first bulkhead door and removing ventilation. Sections 2–4 remained sealed for 15 months, while Section 1 was sealed for only 7 months. To remove artificial sources of heat, electrical power to the investigated region was stopped, except for the 12 V batteries used to power the data loggers and sensors.

b. Monitoring of in-drift microclimate in faulted and nonfaulted zones

Humidity and temperature were measured (Model HMP45C, Campbell Scientific Inc., Logan, Utah) in the isolated Sections 1–4 of the CD, and in a non-isolated section (at Station 15+00) where engineered ventilation remained active.

Electrical resistance probes (ERPs) were used to monitor changes in water content along 200 m of the drift at high spatial and temporal resolution. Working under the principle that the water saturation of a material is inversely proportional to the electrical resistance (Archie, 1942; Blasch et al., 2002), Salve et al. (2000) developed ERPs that use filter paper as the sensing element, such that the electrical resistance depends on the amount of water adsorbed on the filter paper. Individual sensors included two electrical leads located between pieces of filter paper. The probes were square, with 0.01 m sides. Electrical resistance in each probe was determined through a half-bridge measurement. Here, a reference resistor with resistance R_f was introduced into the circuit to facilitate measurement of resistance across the sensing surface (R_s). A known voltage (V_i) was supplied to each sensor for a settling time of 0.1 s before the output voltage (V_x) was measured across the sensors. Using this configuration, the sensor resistance was calculated to be (Campbell Scientific, 1997):

$$R_s = R_f \frac{X/V_x}{1 - X/V_x} \qquad (1)$$

where:

$$X = V_x \left(\frac{R_s}{R_s + R_f} \right) \qquad (2)$$

Resistance was measured from each probe with a datalogger (Model CR10X, Campbell Scientific Inc., Logan, Utah). To make measurements from a large number of sensors, we used multiplexers (Model A416, Campbell Scientific Inc., Logan, Utah) that were connected to the datalogger. Each multiplexer had the capacity to house 48 sensors. To prevent interference between sensors, we measured only one sensor at a time, during which the circuit remained open for all other sensors. All sensors were measured at two hour intervals. An internal check of the measurement system was continuously provided by precision resistors (described below) located randomly on the measurement ports of the multiplexers. Typically, the standard deviations of the errors in the 1 kΩ and 100 kΩ precision resistor measurements were 0.001 and 0.005 kΩ, respectively.

Placed close to the floor of the tunnel and exposed to the in-drift atmosphere, a total of 396 ERPs were installed at 0.5 m intervals between Stations 24+00 (in Section 2) and 26+00 (at the end of Section 3). To keep water from pooling on or near the probes and influencing subsequent measurements, the ERPs were mounted on the outer curved surface of PVC pipes that were sectioned length-wise.

The ERP data were compared with data from co-located relative humidity (RH) sensors (Model HMP 45C, Campbell Scientific Inc., Logan, Utah). The relationship between these two data types is as follows: an increase in relative humidity, as measured by the RH sensor, causes an increase in water saturation of the ERP filter paper, resulting in a decrease in electrical resistance, as measured by the ERPs. Figure 2 compares the ERP and RH response at two locations, focusing on the RH range of 90%–100% (values below this are of less interest as they reflect conditions in which humidity is unnaturally

low due to the engineered ventilation). Comparing collocated EPRs and RH sensors suggests that most of the measured variability in RH at time scales of several days to months is tracked by the ERPs, and that within the 90–100% relative humidity range, the logarithm of the ERP resistance is roughly linearly proportional to the relative humidity.

IV. Observations

a. Temperature and relative humidity

Temperature and RH measurements for Sections 1–4 are presented in Figure 3. After the ventilation was turned off in Sections 2–4 in mid-November 2001, the temperature rapidly decreased for ~1 week, and continued to gradually decrease thereafter (Figure 3A). RH measurements show that humidity in the four nonventilated sections began to increase after the bulkhead doors were closed and ventilation was stopped (Figure 3b). Similar to the temperature responses, the RH initially changed rapidly (increasing in this case), followed by a continued gradual increase. In Section 1 (at Station 21+40), after the section was sealed in December 2001, there were initially rapid changes in a period of two weeks, with values rising from ~10% to ~90%. In the following 5 months, the RH continued to rise, but was interrupted at weekly intervals, likely affected by the adjacent non-isolated section of the drift, for which ventilation was active Monday through Thursday and inactive Friday through Sunday of each week. Deeper in the CD (in Sections 2–4), the average RH response was almost identical with the RH increasing rapidly to ~90% and then gradually toward 100%.

Note that we observed no correlation between the barometric pressure (not shown) and the temperature and RH data.

b. Electrical resistance probes (ERPs)

After the engineered ventilation was removed, ERP resistance values began to rapidly decrease from initial readings at or near the resistance probe maximum of 1000 kΩ to values around 100–1000 kΩ after several months (Figure 4a). We interpret this as the response of the probes to an increase of humidity to near-saturated values, as also measured directly by the humidity sensors (Figure 3b). About 10% (38/396) of the probes did not show this decrease in resistance, but instead continued to give resistance readings close to the maximum value; we assume that this reflects faulty detectors or improper configuration of these probes, and therefore exclude them from our analysis. We also use median rather than mean values when comparing average readings of groups of probes in order to make our analysis less sensitive to possible erratic readings from a few ERPs.

The decrease in the nonfaulted zone (Stations 24+00 to 25+03) was generally faster than in the faulted zone (Stations 25+03 to 26+00), with the initial ten-fold drop in resistance taking a median of 16.4±1.2 and 29.8±2.0 days, respectively. (The uncertainties given are 95% confidence intervals estimated using the bootstrap method.) After the initial decrease, the resistance in the nonfaulted zone remained mostly uniform at low values (i.e., indicating wetter conditions) compared to the faulted section with initially higher values (i.e., indicating drier conditions with less condensation) and more variability. Thus, for March–August 2002, the median EPR resistance in the nonfaulted zone was 407±1 kΩ, compared with 730±2 kΩ in the faulted zone; after August 2002, the difference in median resistance between the sections was smaller (310±1 vs. 455±1 kΩ), but the variability of resistance within the faulted zone continued to be greater than in the

unfaulted zone (Figure 5). Variability in both zones tended to increase with time after decreasing during the initial equilibration period (Figure 5).

Within the nonfaulted section, small differences in the general pattern were noted between January and August 2002, when the region between Stations 24+00 and 24+20 remained drier than the rest of the nonfaulted zone (median: 556±2 vs. 456±1 kΩ). By September 2002, these differences disappeared, but others began to emerge. Resistances were relatively low in the stretch between Stations 24+20 and 24+40 (median: 283±1 kΩ compared with 323±1 kΩ for the rest of the unfaulted section over the same period). In particular, near Station 24+35, there was a large decrease in resistance extending over several meters, which persisted until the end of monitoring. However, for the remainder of this section (Stations 24+40 to 25+03) the resistance remained relatively uniform following the initial decrease.

As in the nonfaulted section, there was no identifiable spatial trend in the faulted section during the first few months. However, by April 2002, for a period of about two months, the faulted section shows a trend going from lower to higher resistance (higher to lower saturation) with increasing station number (median: 569±2 kΩ for Stations 25+03 to 25+60, compared with 905±3 kΩ for Stations 25+60 to 26+00). This spatial pattern was interrupted in early July 2002, when a substantially wetter zone developed between Stations 25+65 and 25+75 and persisted until the end of monitoring (median: 120±1 kΩ for Statiosn 25+65 to 25+75 compared with 489±1 kΩ for the rest of the faulted zone).

The resistance profile is shown in Figure 4b for two times during the monitoring period. Note that for the earlier time the spatial fluctuations are relatively minor, and a trend of increasing resistance is seen in the faulted zone (Stations 25+03 to 26+00).

While the later profile shows similarly mild fluctuations in the nonfaulted zone (except near Station 24+35), more extreme fluctuations are seen in the faulted zone.

Spectral (Lomb periodogram) analysis of the ERP measurement time series showed that most spectral power was at low frequencies of the same order as the total observation period (seasonal or annual time scales). There was no significant diurnal or weekly periodicity.

We tentatively attribute the broad patterns of variation found with ERPs within the faulted zone and the differences between the faulted and unfaulted zone to the penetration of relatively warm, dry air into the fractured zone in the initial months, followed by the localized penetration of moisture near Station 25+70, presumably via a fault, during the latter half of the observation period. Unmapped fractures that convey heat and/or moisture are also a possible explanation for the small-scale variability in ERP readings seen within the ostensibly unfaulted zone, for example near Station 24+35 (Figure 4).

V. Discussion and Conclusion

When engineered ventilation is suppressed in excavated cavities that are thought to be isolated from atmospheric dynamics, it is tempting to assume that a low-energy environment with a stable internal microclimate exists (e.g., De Freitas and Littlejohn, 1987; Gamble et al., 2000). However, our observations suggest that in cavities located in fractured/faulted rock, such as the CD at Yucca Mountain, the microclimatic regime is dynamic and may vary in space and time.

The following observations can be made from this study:

1. A low-cost, high-resolution sensor system has the potential to identify and monitor microclimate dynamics on spatial and temporal scales that are relevant

for the assessment of long-term impacts of condensation on underground facilities.

2. The ERP response suggests that there are changes in condensation patterns within the drift over the spatial scale (200 m) and time frame (~14 months) that we examine. Some areas of the drift are subject to greater amounts of condensation than others.
3. There are significant differences in the microclimates of the faulted and nonfaulted sections, with the faulted section showing greater variability.

While qualitative in nature—since we base our inferences on trends seen in a large number of ERPs that were not calibrated specifically to provide water content or RH estimates—the results of this study point to the need for detailed, quantitative investigation of in-drift microclimates whenever designing or maintaining facilities in fractured, partially saturated rocks.

Acknowledgments

This work was supported by the Director, Office of Civilian Radioactive Waste Management, U.S. Department of Energy, through Memorandum Purchase Order QA-B004220RB3X between Bechtel SAIC Company, LLC, and the Ernest Orlando Lawrence Berkeley National Laboratory (Berkeley Lab). The support is provided to Berkeley Lab through the U.S. Department of Energy Contract No. DE-AC03. . NYK was supported by a National Oceanic and Atmospheric Administration Climate and Global Change Postdoctoral Fellowship. Reviews by Paul Cook, and Dan Hawkes are gratefully acknowledged.

References

Archie GE. 1942. The electrical resistivity log as an aid in determining some reservoir characteristics, *Trans. AIME* 146:54–62.

Blasch KW, Ferre TPA, Christensen AH, Hoffmann JP. 2002. New field method to determine streamflow timing using electrical resistance sensors, *Vadose Zone J.*, 1: 289–299.

Campbell Scientific, Inc., CR10X Measurement and control system, operators manual, 1997.

Crouzeix C, Le Mouël JL, Perrier F, Richon P, Morat P. 2003. Long-term thermal evolution and effect of low power heating in an underground quarry, *Comptes Rendus Geoscience*, 335: 345–354.

De Freitas CR, Littlejohn RN. 1987. Cave climate: Assessment of heat and moisture exchange, *J. of Climatology*, 7: 553–569

De Freitas CR, Schmekal A. 2003. Condensation as a microclimate process: measurement, numerical simulation and prediction in the Glowworm Cave, New Zealand, *Int. J. Climatol.* 23: 557–575.

Gamble DW, Dogwiler JT, Mylroie J. 2000. Field assessment of the microclimatology of tropical flank margin caves, *Climate Research*, 16: 37-50.

Mongano GS, Singleton WL, Moyer TC, Beason SC, Eatman GLW, Albin AL, Lung RC. 1999. Geology of the ECRB Cross Drift-Exploratory Studies Facility, Yucca Mountain Project, Yucca Mountain, Nevada, Bureau of Reclamation and U.S. Geological Survey, Denver, Colorado.

Piety LA. 1996. Compilation of known or suspected Quaternary faults within 100 km of Yucca Mountain, OF 94-0112, USGS, Denver, CO.

Salve R, Wang JSY, Tokunaga TK. 2000. A probe for measuring wetting front migration in rocks, *Water Resour. Res*., 36: 1359–1367.

Stuckless JS, Dudley WW. 2002. The geohydrologic setting of Yucca Mountain, Nevada, *Appl. Chem*., 17: 659–682.

Figure Captions

Figure 1. (A) Cross section of Yucca Mountain showing the geology of the formation surrounding the Cross-Drift (CD). The 'x' axis indicates the distance in meters along the tunnel from the point of entry (i.e. 0+00 m), and the 'y' axis is the elevation in meters above mean sea level. (B) Location of the four bulkhead doors used to isolate sections of the drift from engineered ventilation. (C) Photograph of the Solitario Canyon Fault in Section 3 of the drift.

Figure 2. Comparison of in-drift electrical resistance probe (ERP) measurements with relative humidity measurements made using commercially available probes (Model HMP 45C, Campbell Scientific, Logan, Utah). The insets depict expanded views over a time period of two weeks. Note in (A) there is significant deviation between the RH and ERP measurements past approxiamtely mid-July 2002. This reflects malfunctioning of the RH sensor from this time onward.

Figure 3. (A) Temperature and (B) relative humidity measured at four locations in the CD. The legend indicates the locations of the sensors along the drift. A drop in temperature just before December 6, 2002 in Section 3 results from the battery losing adequate power.

Figure 4. Resistance data collected with ERPs from Stations 24+00 to 26+00. (A) Data collected at all times with color representing resistance (in kΩ). B) Resistance profile at two times, as indicated by dashed lines in (A).

Figure 5. Comparison of spatial variability in probe resistance (median absolute deviation, 8-day moving average) between the faulted and unfaulted zones (Sta. 24+00 to

25+03 and 25+03 to 26+00 respectively). The thin dashed curves indicate the 95% confidence interval. Except for the very beginning period, variability is consistently greater in the faulted zone

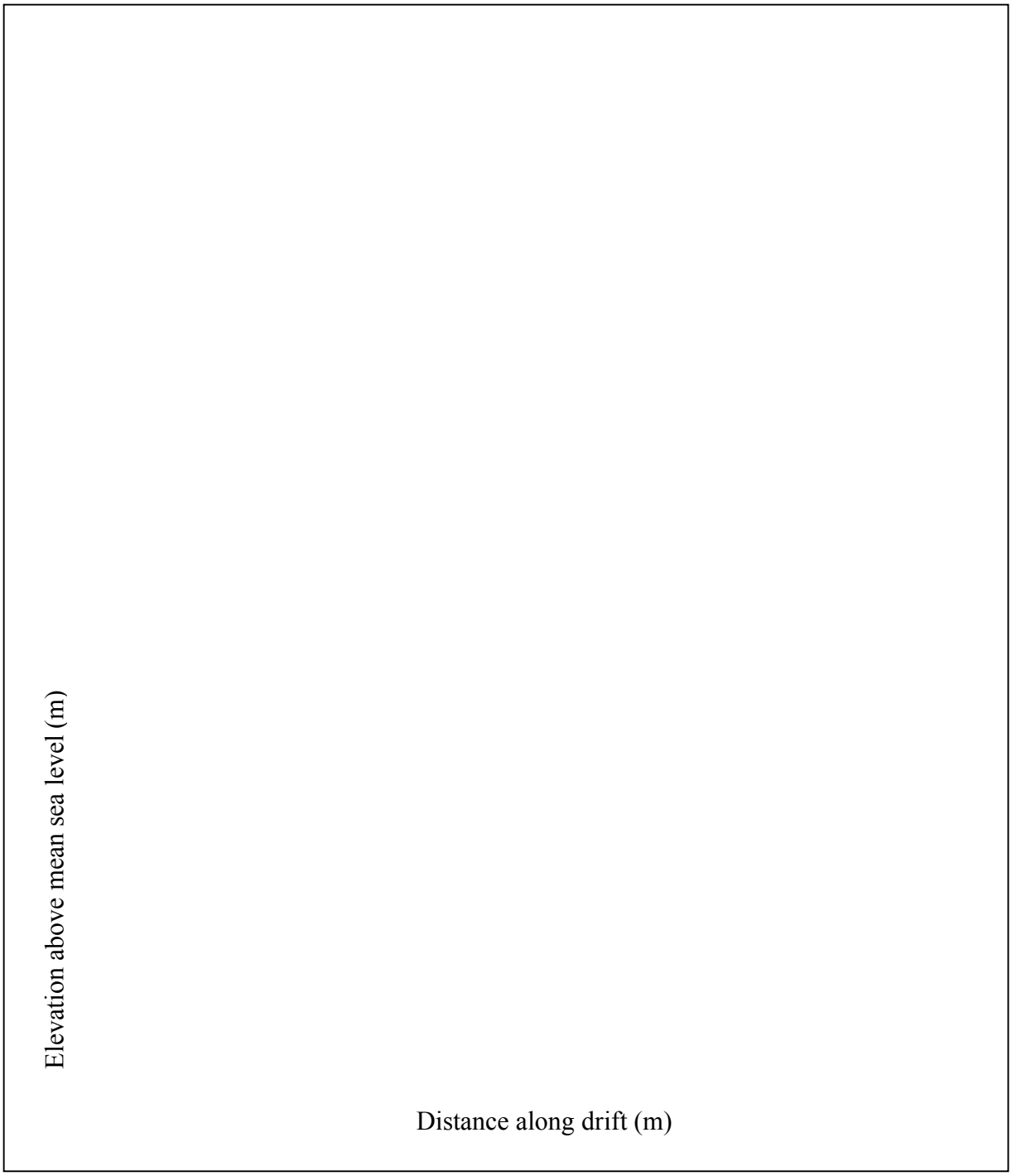

Figure 1.

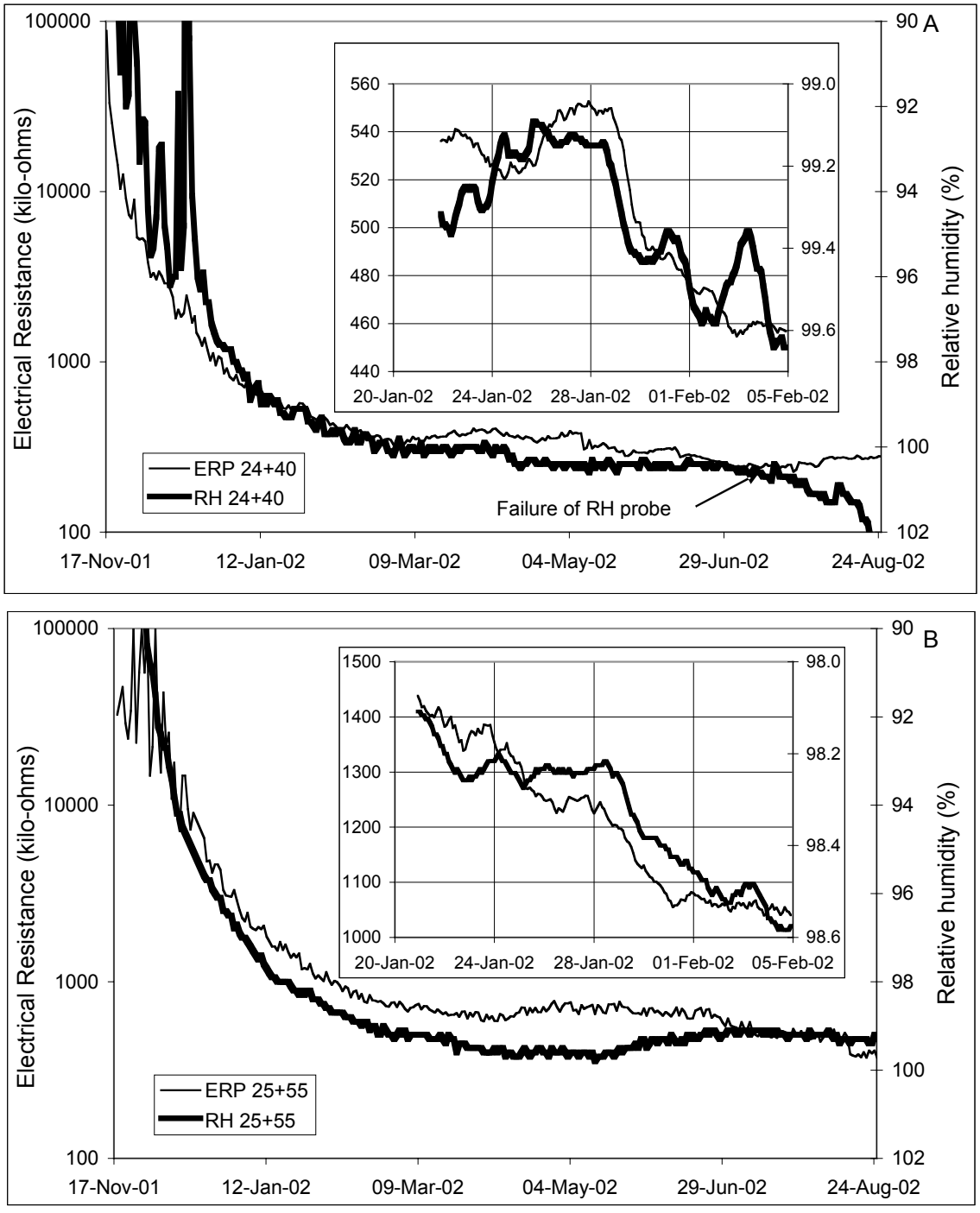
A
Electrical Resistance (kilo-ohms)
Relative humidity (%)
100000
10000
1000
100
90
92
94
96
98
100
102
17-Nov-01
12-Jan-02
09-Mar-02
04-May-02
29-Jun-02
24-Aug-02
ERP 24+40
RH 24+40
Failure of RH probe
560
540
520
500
480
460
440
99.0
99.2
99.4
99.6
20-Jan-02
24-Jan-02
28-Jan-02
01-Feb-02
05-Feb-02
B
Electrical Resistance (kilo-ohms)
Relative humidity (%)
100000
10000
1000
100
90
92
94
96
98
100
102
17-Nov-01
12-Jan-02
09-Mar-02
04-May-02
29-Jun-02
24-Aug-02
ERP 25+55
RH 25+55
1500
1400
1300
1200
1100
1000
98.0
98.2
98.4
98.6
20-Jan-02
24-Jan-02
28-Jan-02
01-Feb-02
05-Feb-02

Figure 2.

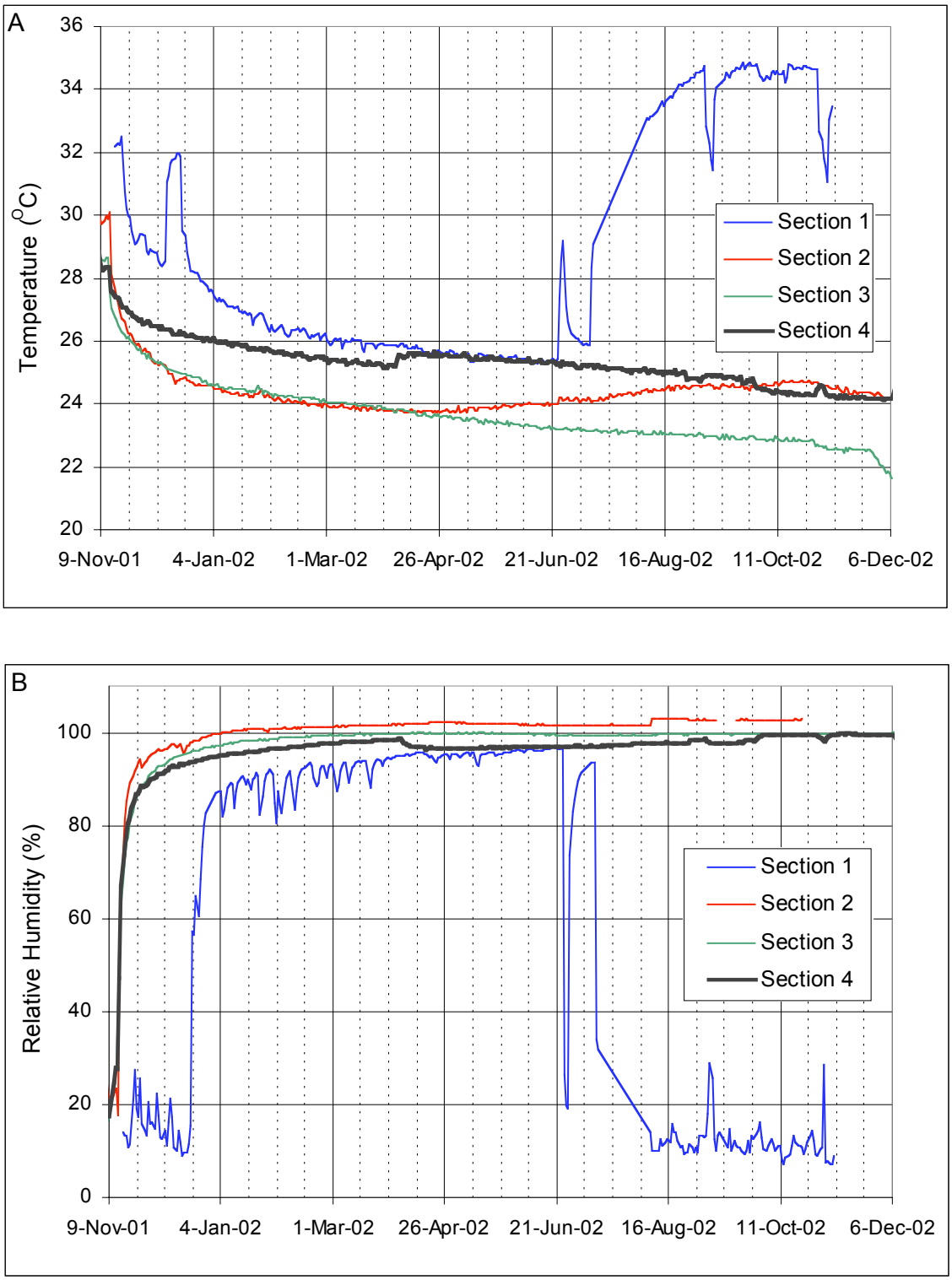
A
Temperature (°C)
36
34
32
30
28
26
24
22
20
9-Nov-01
4-Jan-02
1-Mar-02
26-Apr-02
21-Jun-02
16-Aug-02
11-Oct-02
6-Dec-02
Section 1
Section 2
Section 3
Section 4
B
Relative Humidity (%)
100
80
60
40
20
0
9-Nov-01
4-Jan-02
1-Mar-02
26-Apr-02
21-Jun-02
16-Aug-02
11-Oct-02
6-Dec-02
Section 1
Section 2
Section 3
Section 4

Figure 3.

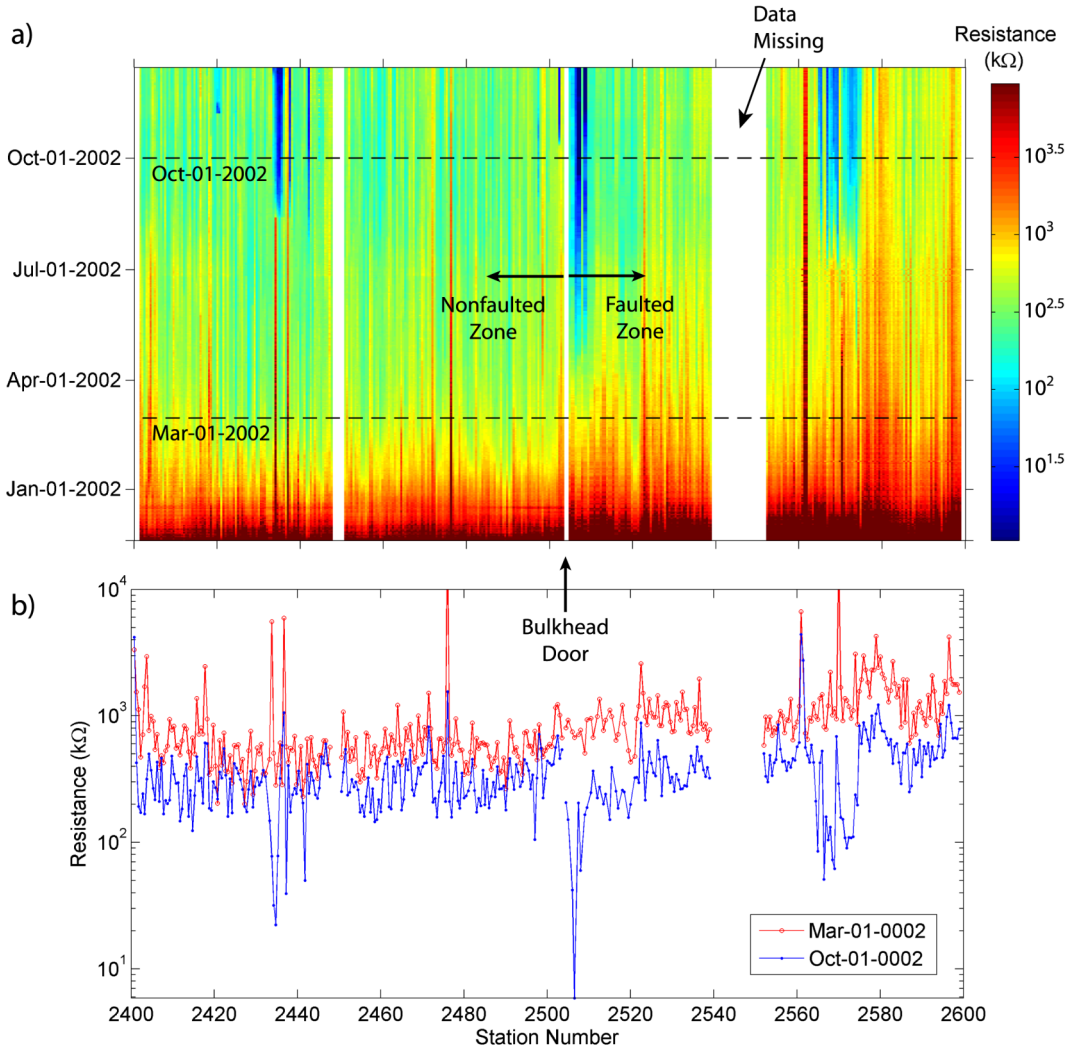
a)
Data
Missing
Resistance
(kΩ)
Oct-01-2002
Oct-01-2002
Jul-01-2002
Nonfaulted
Zone
Faulted
Zone
Apr-01-2002
Mar-01-2002
Jan-01-2002
$10^{3.5}$
10^{3}
$10^{2.5}$
10^{2}
$10^{1.5}$
b)
Bulkhead
Door
Resistance (kΩ)
10^{4}
10^{3}
10^{2}
10^{1}
Mar-01-0002
Oct-01-0002
2400
2420
2440
2460
2480
2500
2520
2540
2560
2580
2600
Station Number

Figure 4.

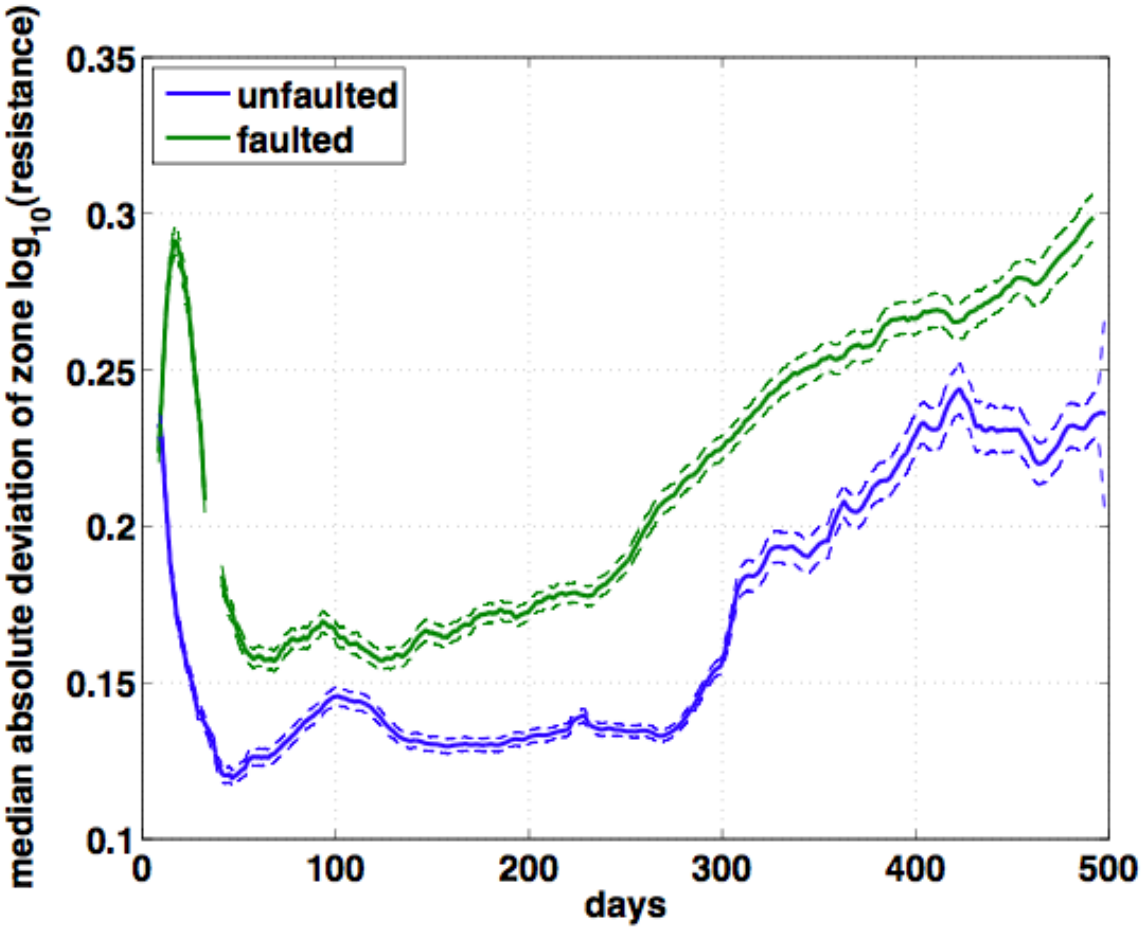
unfaulted
faulted
median absolute deviation of zone log10(resistance)
0.35
0.3
0.25
0.2
0.15
0.1
0
100
200
300
400
500
days

Figure 5.